

Non-LTE line formation for Si I- II- III in A-B stars and the origin of Si II emission lines in ι Her

Lyudmila Mashonkina,¹[★]

¹*Institute of Astronomy of the Russian Academy of Sciences, Pyatnitskaya st. 48, 119017, Moscow, Russia*

Accepted XXX. Received YYY; in original form ZZZ

ABSTRACT

A comprehensive model atom was developed for Si I- II- III using the most up-to-date atomic data available so far. Based on the non-local thermodynamic equilibrium (NLTE) line formation for Si I, Si II, and Si III and high-resolution observed spectra, we determined the NLTE abundances for a sample of nine unevolved A9 to B3-type stars with well determined atmospheric parameters. For each star, NLTE reduces substantially the line-to-line scatter for Si II compared with the LTE case and leads to consistent mean abundances from lines of different ionisation stages. In the hottest star of our sample, ι Her, Si II is subject to overionisation that drives emission in the lines arising from the high-excitation doublet levels. Our NLTE calculations reproduced 10 emission lines of Si II observed in ι Her. The same overionisation effect leads to greatly weakened Si II lines, which are observed in absorption in ι Her. Large positive NLTE abundance corrections (up to 0.98 dex for 5055 Å) were useful for achieving consistent mean abundances from lines of the two ionisation stages, Si II and Si III. It was found that the NLTE effects are overestimated for the Si II 6347, 6371 Å doublet in ι Her, while the new model atom works well for the cooler stars. At this stage, we failed to understand this problem. We computed a grid of the NLTE abundance corrections for lines of Si I, Si II, and Si III in the model atmospheres with effective temperatures and surface gravities characteristic of unevolved A-B type stars.

Key words: line: formation – stars: abundances – stars: atmospheres.

1 INTRODUCTION

Silicon is one of the most abundant metals. Analyses of the silicon lines in A- to mid B-type stars are important for addressing several problems. Such stars are young and can serve as indicators for present-day cosmic abundances. Using a sample of unevolved early B-type stars in nearby OB associations and the field and the non-local thermodynamic equilibrium (non-LTE = NLTE) line formation for Si III, Przybilla et al. (2008) and Nieva & Przybilla (2012) establish the Cosmic Abundance Standard and prove that the mean stellar silicon abundance agrees within 0.01 dex with the solar one. Fossati et al. (2009) investigate whether the chemical composition of the solar photosphere can be regarded as a reference also for early A and late B-type stars. For each of their three stars, the LTE analysis led to quite discordant abundances from lines of different ionisation stages of silicon. Fossati et al. (2009) claim the real need of calculations based on the NLTE line formation for Si I - Si II - Si III in A to mid B-type stars.

Exactly in this range of spectral types, spectroscopic peculiarities (chemical abundance peculiarities, stratification, Zeeman effect, etc.) are frequent for stars. In order to correctly quantify the impact of the various physical processes that occur inside the atmospheres of such stars on the emergent spectra, one needs to test how the applied methods of spectral analysis allow one to fit the observations. Bailey & Landstreet (2013) determine the LTE abundances from lines of the first and second ions of silicon in magnetic Bp and HgMn stars and use normal B stars of similar temperatures as a comparison sample. Both magnetic and non-magnetic stars show a discordance between the Si II and Si III based abundances, however, the effect is much smaller for the normal B-type stars, with the abundance difference $\text{Si III} - \text{Si II} = 0.3$ to 0.8 dex for different stars. The departures from LTE are suggested as a source of these discrepancies.

In A to mid B-type stars, silicon can be observed in lines of the two ionisation stages: Si I and Si II, if the star's effective temperature (T_{eff}) is below approximately 11 000 K, and Si II and Si III for the hotter stars. This is suitable for constraining and checking atmospheric parameters. For different temperatures, either Si I or Si II is a minority species, for which the statistical equilibrium (SE) can easily deviate

★ E-mail: lima@inasan.ru

from thermodynamic equilibrium owing to deviations of the mean intensity of ionising radiation from the Planck function. Therefore, a correct evaluation of atmospheric parameters from the Si I/Si II or Si II/Si III ionisation equilibrium method can only be possible, when neglecting the LTE assumption.

Sadakane & Nishimura (2017, 2019) registered weak emission lines of Si II in the red-region spectra of slowly rotating early B-type stars, and HD 160762 (ι Her, B3 IV) among them. The LTE calculations with classical hydrostatic model atmosphere can only yield an absorption line profile, but never the emission one. Mihalas et al. (1972) were the first who showed that the emission line (N III 4634, 4640, 4641 Å) in spectra of the main-sequence objects (O stars with $T_{\text{eff}} \geq 37000$ K) can be reproduced using classical hydrostatic model atmospheres, when taking the NLTE effects on the line formation into account. In ι Her, emission lines are observed for several chemical species (Sadakane & Nishimura 2019). For C I and Ca II, their emission lines are well reproduced in the NLTE calculations of Alexeeva et al. (2016) and Sitnova et al. (2018), respectively.

Non-LTE effects for Si I (and Si II, in some cases) are studied broadly for late-type and low-metallicity stars, using the model atoms treated by Vernazza et al. (1976); Finn & McAllister (1978); Shi et al. (2008); Bard & Carlsson (2008); Shchukina et al. (2012); Bergemann et al. (2013), and Amarsi & Asplund (2017). At the hottest end of spectral type sequence, early B and O, NLTE calculations for Si II, Si III, and Si IV are performed with the model atoms constructed by Kamp (1978); Lennon et al. (1986), and Becker & Butler (1990). As for A to mid B-type stars, very few estimates of the NLTE abundances are based on theoretical results of Wedemeyer (2001), who studied the Si II 3862, 4128-30, and 5041-56 Å lines in a benchmark star Vega.

This study aimed to fill a gap in theoretical research of the line formation in stellar atmospheres and to develop the NLTE method for analysis of the Si I, Si II, and Si III lines in spectra of A to mid B-type stars. For a sample of nine unevolved A9 to B3-type stars with well determined atmospheric parameters, we investigated whether we can obtain for each star consistent abundances from different lines of silicon in different ionisation stages. A challenge for this study was understanding an origin of the Si II emission lines in ι Her.

The paper is organised as follows. The new model atom for Si I-II-III is presented in Sect. 2. Our stellar sample, observational material, and the adopted atmospheric parameters are described briefly in Sect. 3. The NLTE effects on atomic level populations and lines of Si I, Si II, and Si III are discussed in Sect. 4. Section 5 presents the abundance results for eight stars with $T_{\text{eff}} \leq 12800$ K. Section 6 is devoted to our hottest star, ι Her, with its emission lines of Si II. Having convinced that the NLTE method works well for Si I-II-III through a range of A-B spectral types, we compute in Sect. 7 the NLTE abundance corrections for the silicon lines in the grid of model atmospheres. Our conclusions are summarised in Sect. 8.

2 MODEL ATOM OF SI I-SI II-SI III

Energy levels. For Si I we employ all the 451 energy levels below the ionisation threshold, $\chi_{\text{thr},1} = 65736.06 \text{ cm}^{-1} = 8.187 \text{ eV}$, provided by the NIST¹ database (Kramida et al. 2019) based on the data of Martin & Zalubas (1983) and also the 268 high-excitation levels, which are predicted by R. Kurucz² in calculations of the Si I atomic structure and which are missing in NIST. The model atom includes the multiplet fine structure for all the terms up to Si I $3p5s^3P^\circ$, with an excitation energy of $E_{\text{exc}} = 6.725 \text{ eV}$. For the $E_{\text{exc}} > 7.96 \text{ eV}$ levels, a combining procedure was applied, if the levels have a common parity and the energy separation does not exceed 0.037 eV (300 cm^{-1}). Thus, 95 levels in our model atom of Si I were made using the NIST data and 23 levels using the Kurucz's predictions.

For Si II and Si III, the same sources of data were used, as for Si I. NIST provides 93 energy levels of Si II below the ionisation threshold, $\chi_{\text{thr},2} = 131838.14 \text{ cm}^{-1} = 16.346 \text{ eV}$. Taking into account the multiplet fine structure for the Si II ground ($3p^2P^\circ$) and first excited ($3p^24P$) terms and neglecting it for all the other terms, we obtained 50 levels. We also implemented the 28 high-excitation levels predicted by R. Kurucz, which were combined into six levels. Our model atom of Si II is complete up to principal quantum number $n = 9$ and orbital quantum number $l = 7$ and includes the terms with $l \leq 4$ for $n = 10$ and 11.

For Si III, NIST provides 177 energy levels of the $3snl$ ($n \leq 9, l \leq 8$) and $3pnl$ ($n \leq 4, l \leq 2$) electronic configurations. Neglecting the multiplet fine structure for all the terms except the first excited one, $3p^3P^\circ$, we obtained 54 levels in the model atom of Si III.

For $T_{\text{eff}} < 10000$ K, the NLTE calculations were performed with a reduced model atom, which includes levels of Si I, Si II, and the ground state of Si III, because, in such atmospheres, a fraction of Si III is small and no Si III line can be detected in the $T_{\text{eff}} < 10000$ K stars. For the higher temperatures, we used a model atom that includes four ionisation stages, that is Si I, Si II, Si III, and the ground state of Si IV.

Radiative bound-bound (b-b) transitions. We do not take into account radiative transitions with either a wavelength of $\lambda > 300000 \text{ Å}$ or oscillator strength of $f_{lu} < 10^{-6}$. Finally, radiative rates were computed for 1814, 475, and 327 allowed transitions of Si I, Si II, and Si III, respectively. Their f_{lu} -values were taken from calculations of R. Kurucz. In case, if either lower or/and upper level of the transition is combined, the average-“multiplet” oscillator strength was calculated as $f_{lu} = \Sigma g_i f_{ij} / g_l$, where summing is performed for all the levels i and j , which constitute the levels l and u , respectively; g_i and g_l are the statistical weights of the levels i and l .

Radiative bound-free (b-f) transitions. For 55 lowest levels of Si I with angular momentum $L \leq 3$, up to $3p7s^3P^\circ$ (the threshold wavelength is $\lambda_{\text{thr}} = 24000 \text{ Å}$), 41 levels of Si II ($L \leq 4$, up to $9p^2P^\circ$ with $\lambda_{\text{thr}} = 14690 \text{ Å}$), and 40 levels of Si III up to $7d^3D$ ($\lambda_{\text{thr}} = 4742 \text{ Å}$), we rely on the photoionisation cross sections calculated within the Opacity Project (OP, Seaton 1987) and accessible in the TOPbase³ database

¹ <https://physics.nist.gov/PhysRefData/ASD>

² <http://kurucz.harvard.edu/atoms/>

³ <http://cdsweb.u-strasbg.fr/cgi-bin/topbase/>

(Cunto et al. 1993). For the remaining levels in the model atom, the hydrogenic approximation was used with effective principal quantum number n_{eff} instead of n .

We note that the photoionisation cross sections computed by Nahar (2000) and Nahar (1995) for Si I and Si II, respectively, as available in the NORAD⁴ database, are very similar to the TOPbase's ones for photon energies close to the ionisation threshold within approximately 0.5 Ryd, and they are systematically smaller at the higher photon energies, by 0.1 to 0.5 dex for different levels. Singh et al. (2011) calculated for the first time the photoionisation cross sections for the fine-splitting levels of the Si II $3s^23p^2P^\circ$, $3s3p^2^4P$, and $3s3p^2^2D$ terms. Since these data are not available in a tabular form, they cannot be checked in our NLTE calculations. However, we note that in the stellar parameter range, with which this study concerns, photoionisation of the $3s^23p^2P^\circ$ and $3s3p^2^4P$ terms affects only weakly the SE of Si II. For Si II $3s3p^2^2D$, the photoionisation cross sections in Figures 6 and 7 of Singh et al. (2011) are smaller than the TOPbase ones for photon energies below 1.2 Rydberg and resemble predictions of Nahar (1995).

Collisional transitions. For Si I the electron-impact excitations are not yet known with sufficient accuracy, and our calculations of collisional rates rely on theoretical approximations. We used the formula of van Regemorter (1962) for the allowed transitions and assumed that the effective collision strength $\Upsilon = 1$ for the forbidden transitions. For 414 transitions between the terms up to $3s3p3d^2P^\circ$ in Si II (28% of the total number of collisional transitions in Si II) and 210 transitions between the terms up to $3p3d^1F^\circ$ in Si III (15% of the total number of collisional transitions in Si III), we employed the data from the R-matrix calculations of Aggarwal & Keenan (2014) and Fernández-Mencheró et al. (2014), respectively. The same formulas as for Si I were applied for the remaining transitions in Si II and Si III. Ionisation by electronic collisions was calculated everywhere from the Seaton (1962) formula with the hydrogenic photoionization cross section at threshold.

The effects of uncertainties in atomic data on the NLTE results are discussed in Sect. 6, using the silicon emission and absorption lines in ι Her.

3 STELLAR SAMPLE, OBSERVATIONS, ATMOSPHERIC PARAMETERS

As a test and first application of the model atom, silicon lines in nine objects were analysed. This research continues a series of the NLTE studies of chemical species in A-B type stars, namely, O I (Sitnova et al. 2013), C I-II (Alexeeva et al. 2016), Ti I-II (Sitnova et al. 2016), Mg I-II (Alexeeva et al. 2018), Ca I-II (Sitnova et al. 2018). Therefore, we take the same stellar sample with their atmospheric parameters and the same spectral observations. The selected stars, their effective temperatures, surface gravities ($\log g$), metallicities ($[Fe/H]$), microturbulent velocities (ξ_t), and the sources of these data are listed in Table 1.

Alexeeva et al. (2016) described in detail the programme stars. We briefly summarise. Only sharp-lined stars,

with rotational velocities of $V \sin i \lesssim 20 \text{ km s}^{-1}$, were included in our sample, in order to do spectral analysis at the highest precision.

The stars 21 Peg and ι Her are chemically normal single stars.

Each of HD 32115, HD 73666, and π Cet is a primary component of single line spectroscopic binary (SB1), with negligible flux coming from the secondary star. Therefore, it is safe to analyse these stars ignoring the presence of their secondaries. For none of them, a chemical peculiarity was reported. HD 73666 is a Blue Straggler and a member of the Praesepe cluster.

HD 145788 reveals an overabundance of almost all metals, according to Fossati et al. (2009). They conclude that its element abundance pattern 'could be explained if HD 145788 was formed in a region of the sky with a metallicity higher than the solar region'.

Sirius is an astrometric visual binary system composed of a main-sequence A1V star and a DA white dwarf. The primary component is classified as a metallic-line (Am) star.

HD 72660 was classified by Golriz & Landstreet (2016) as a transition object between an HgMn star and an Am star.

Vega is a rapidly rotating star seen pole-on and is also classified as a mild λ Bootis-type star. Similarly to our previous studies, we ignore the non-spherical effects and analyse Vega's flux spectrum using the average temperature and gravity.

We refer to the original papers and also Alexeeva et al. (2016, 2018), and Sitnova et al. (2016) for a description of the methods of atmospheric parameter determinations.

For the seven of nine stars, observational material for the visual spectral range was obtained with a spectral resolving power of $R = \lambda/\Delta\lambda > 60\,000$ and a signal-to-noise ratio of $S/N > 200$, using the ESPaDOnS instrument of the Canada-France-Hawaii Telescope (CFHT). Vega was observed by A. Korn using the spectrograph FOCES ($R \approx 40\,000$, $S/N > 750$) at the 2.2 m telescope of the Calar Alto Observatory. HD 145788 was observed with the échelle spectrograph HARPS instrument ($R \approx 115\,000$, $S/N \approx 200$) attached at the 3.6-m ESO La Silla telescope. For HD 72660, we use also the UV spectrum kindly provided by J. Landstreet. The observations and spectrum reduction are described by Golriz & Landstreet (2016).

4 NON-LTE CALCULATIONS

4.1 Codes, model atmospheres, list of investigated lines

The coupled radiative transfer and SE equations were solved with a modified version of the DETAIL code (Butler & Giddings 1985; Przybilla et al. 2011). As verified by Przybilla et al. (2011), a hybrid method combining LTE atmospheres and NLTE line formation is able to reproduce observations for effective temperatures between 15 000 and 35 000 K. This is all the more true for cooler atmospheres. For consistency with our earlier studies, for each star we used exactly the same model atmosphere. Classical plane-parallel and LTE model atmospheres were calculated with the code

⁴ <https://norad.astronomy.osu.edu/>

Table 1. Atmospheric parameters of the sample stars and mean NLTE (N) and LTE (L) abundances from lines of different ionisation stages of silicon.

HD	T_{eff} [K]	log g	[Fe/H]	ξ_t	Ref	Si I		Si II		Si III		[Si/H]	
						N_l	log ϵ	N_l	log ϵ	N_l	log ϵ		
32115	7250	4.20	0.00	2.3	F11	N	16	7.58(0.17)	4	7.65(0.08)		0.10	
						L		7.61(0.17)		7.82(0.24)			
73666 (40 Cnc)	9380	3.78	0.10	1.8	F07	N	1	7.54	13	7.68(0.17)		0.10	
						L		7.16		7.84(0.26)			
172167 (Vega)	9550	3.95	-0.50	1.8	C93	N			8	6.92(0.15)		-0.59	
						L				7.08(0.17)			
72660	9700	4.10	0.40	1.8	S16	N	6	7.85(0.04)	14	7.82(0.11)		0.33	
						L		7.59(0.09)		7.94(0.23)			
145788	9750	3.70	0.46	1.3	F09	N			7	7.63(0.12)		0.12	
						L				7.90(0.19)			
48915 (Sirius)	9850	4.30	0.40	1.8	H93	N	1	7.59	11	7.72(0.11)		0.21 ¹	
						L		7.26		7.84(0.18)			
209459 (21 Peg)	10400	3.55	0.00	0.5	F09	N	1	7.49	17	7.50(0.13)		-0.01	
						L		7.08		7.62(0.29)			
17081 (π Cet)	12800	3.75	0.00	1.0	F09	N			19	7.75(0.14)	2	7.72(0.04)	0.23
						L				7.59(0.25)		7.82(0.00)	
160762 (ι Her)	17500	3.80	0.02	1.0	N12	N			13	7.74(0.25) ²	4	7.54(0.07)	0.03 ³
						L				7.07(0.41) ²		7.79(0.05)	

Notes. The numbers in parentheses are the dispersions in the single line measurements around the mean. ξ_t is in km s^{-1} .

¹ based on Si II lines; ² Si II 6347, 6371 Å and emission lines are not accounted in the mean; ³ based on Si III lines.

Ref: C93 = [Castelli & Kurucz \(1993\)](#), F07, F09, F11 = [Fossati et al. \(2007, 2009, 2011\)](#),

H93 = [Hill & Landstreet \(1993\)](#), N12 = [Nieva & Przybilla \(2012\)](#), S16 = [Sitnova et al. \(2016\)](#).

LLMODELS ([Shulyak et al. 2004](#)). For Sirius, its model atmosphere was taken from R. Kurucz website⁵.

Linelists of [Fossati et al. \(2009, 2011\)](#), and [Sadakane & Nishimura \(2019\)](#) were used to select the silicon lines for the non-LTE analysis. A sample of lines observed in stellar spectra changes substantially, when moving from our coolest to the hottest star. Therefore, the used lines together with their atomic parameters are listed in five separate Tables: Si I and Si II lines in HD 32115 (Table 2), Si I UV lines (Table 3), Si I and Si II lines in the visible spectra of eight stars with $T_{\text{eff}} > 9000$ K (Table 4), Si III lines (Table 5), and Si II emission lines in ι Her (Table 7). For lines of Si III, the quadratic Stark effect broadening was taken into account using approximate formula of [Cowley \(1971\)](#).

In this research, analysis of observed spectra is based on line profile fitting. The synthetic spectra were computed with the SYNTHV_NLTE code ([Tsymbal et al. 2019](#)), which implements the pre-computed departure coefficients from the DETAIL code. We note that SYNTHV_NLTE treats a contribution of the overlapping hydrogen Balmer lines to background opacity using the occupation probability theory, as developed by [Hummer & Mihalas \(1988\)](#), [Hubeny et al. \(1994\)](#), and [Nayfonov et al. \(1999\)](#). This is important for calculations of Si I 3905 Å and Si II 3853, 3856, 3862 Å. The best fit to the observed spectrum was obtained automatically using the IDL BINMAG code by O. Kochukhov⁶. The line list and atomic data for the synthetic spectra calculations were taken from the VALD database ([Ryabchikova et al. 2015](#)).

4.2 Statistical equilibrium of silicon depending on effective temperature

For the energy levels, which are important for understanding a formation of the silicon lines, which are observed in our sample stars, Fig. 1 displays the departure coefficients, $b = n_{\text{NLTE}}/n_{\text{LTE}}$, in four model atmospheres with different T_{eff} . Here, n_{NLTE} and n_{LTE} are the statistical equilibrium and thermal (Saha-Boltzmann) number densities, respectively. In our coolest atmosphere ($T_{\text{eff}} / \log g = 7250$ K / 4.20), silicon is strongly ionised, with $N(\text{Si II})/N(\text{Si I}) > 30$. For Si I, the departures from LTE take place above continuum optical depth $\log \tau_{5000} \simeq -1$. Superthermal radiation of a non-local origin below the thresholds of the Si I levels, such as $3p^2\ ^1D$ ($\lambda_{\text{thr}} = 1682$ Å), $3p4s\ ^1P^\circ$ ($\lambda_{\text{thr}} = 4039$ Å), and $3p3d\ ^1D^\circ$ ($\lambda_{\text{thr}} = 5435$ Å), tends to overionise Si I. However, bound-bound transitions from many levels close to the ionisation limit down to the lower levels can siphon an efficient flow of electrons downward. It increases the populations of the ground state, $3p^2\ ^3P$, and low-lying levels, such as $3p^2\ ^1S$ and $3p4s\ ^1P^\circ$, above their thermodynamic equilibrium (TE) values, but depopulates the high-excitation ($E_{\text{exc}} \gtrsim 6$ eV) levels, such as $3p5d\ ^3P^\circ$ (in the top panel of Fig. 1, it is quoted as $5d\ ^3P^\circ$ for brevity). The levels above $3d\ ^2D$ in Si II are underpopulated ($b < 1$) by photon losses in the transitions to the lower levels as soon as the line center optical depth drops below 1. Two transitions from the ground state to $4s\ ^2S$ ($\lambda = 1526, 1533$ Å) are close to be in detailed balance throughout the atmosphere. This explains why population of $4s\ ^2S$ is close to the TE value.

In the hotter model atmosphere (9700/4.10), no processes in Si I can compete with overionisation of the low-lying levels, resulting in strong depopulation of all the Si I

⁵ <http://kurucz.harvard.edu/stars/sirius/ap04t9850g43k0he05y.dat>

⁶ <http://www.astro.uu.se/~oleg/binmag.html>

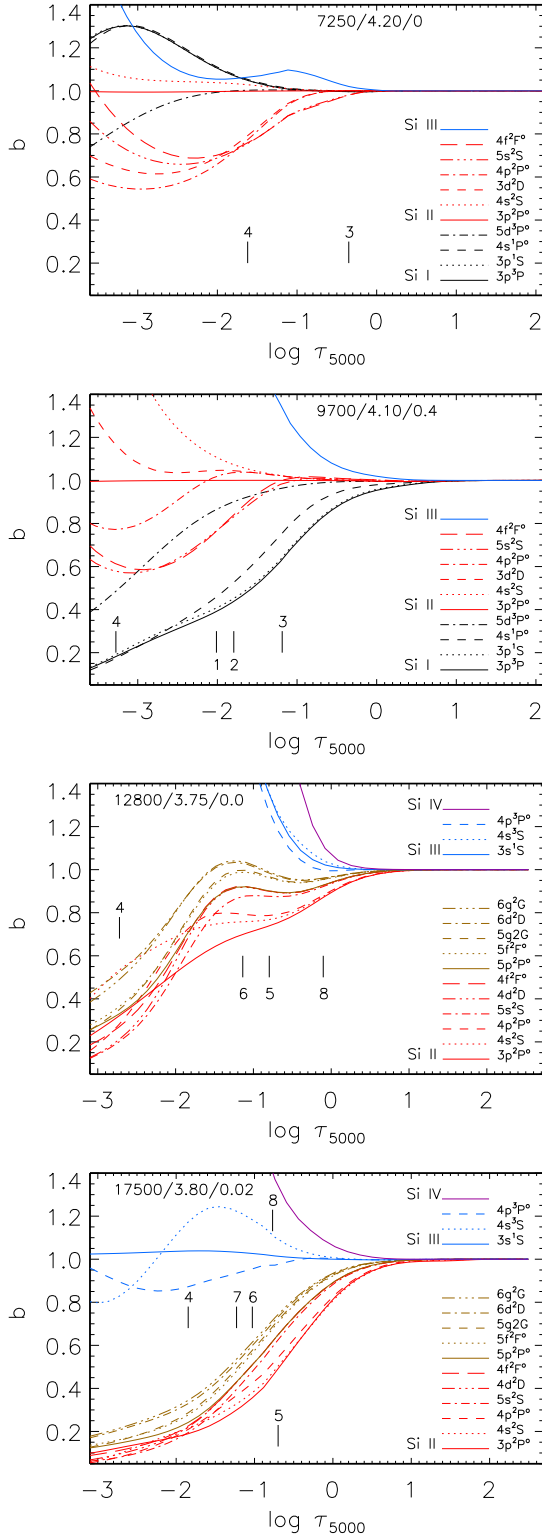


Figure 1. Departure coefficients, b , for the levels of Si I (black curves, two top panels), Si II (red and brown curves), Si III (blue curves), and Si IV (lilac curves) as a function of $\log \tau_{5000}$ in the model atmospheres 7250/4.20/0, 9700/4.10/0.4, 12800/3.75/0.0, and 17500/3.80/0.02. The selected levels are quoted in the right part of each panel. Tick marks indicate the locations of line center optical depth unity for the following lines: Si I 1666 (1) and 3905 Å (2), Si II 5957 (3), 6347 (4), 6239 (5), 7848 (6), and 9412 Å (7) and Si III 4567 Å (8).

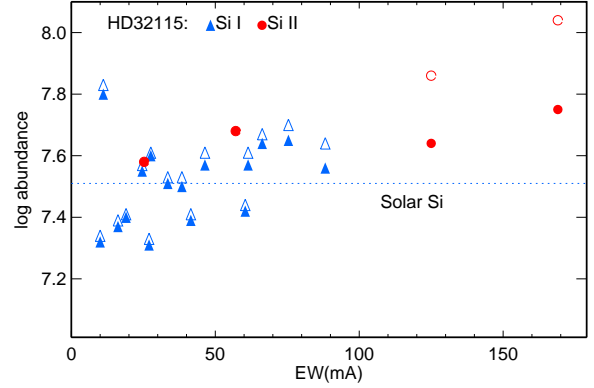


Figure 2. NLTE (filled symbols) and LTE (open symbols) abundances from lines of Si I (triangles) and Si II (circles) in HD 32115.

levels. Si II remains to be a majority species, and its ground state keeps the TE population throughout the atmosphere. Below $\log \tau_{5000} \approx -1$ the most important transitions of Si II are in detailed balance and the departure coefficients of the excited levels are close to 1. In the higher atmospheric layers, strong pumping transitions $3p^2P^o - 4s^2S$ ($\lambda = 1526, 1533$ Å) and $3p^2P^o - 3d^2D$ ($\lambda = 1260, 1264$ Å) produce enhanced excitation of the upper levels, while photon losses in the transitions to low-lying levels depopulate $4p^2P^o$ and the levels above.

Si I is strongly overionised in the two hottest models, 12800/3.75 and 17500/3.80, which represent the atmospheres of π Cet and ι Her. Since no lines of Si I can be measured in these stars, levels of Si I are not shown in Fig. 1. In the 12800/3.75 model, Si II and Si III have comparable number densities in the line-formation layers, above $\log \tau_{5000} = 0$. Superthermal radiation below the thresholds of the Si II levels, such as $4s^2S$ ($\lambda_{\text{thr}} = 1507$ Å), $3d^2D$ ($\lambda_{\text{thr}} = 1905$ Å), and $3p^2P^o$ ($\lambda_{\text{thr}} = 1306$ Å), leads to an overionisation of Si II, but enhanced populations of the Si III levels.

In the 17500/3.80 model, Si II is subject to strong overionisation, while Si III is a majority species. Its ground state keeps close to the TE population throughout the atmosphere. Pumping UV transitions from the low-excitation levels produce enhanced excitation of the lower level of the Si III $4s^3S - 4p^3P^o$ transition (triplet lines at 4552, 4567, and 4574 Å) above $\log \tau_{5000} \approx 0$, while the upper level is depopulated via spontaneous transitions.

4.3 Non-LTE effects on spectral lines

Tables 2, 3, 4, and 5 and Figs. 2 and 3 present the NLTE and LTE abundances from individual lines in the sample stars.

4.3.1 Lines of Si I

The 16 lines of Si I were measured in our coolest star, HD 32115 (Table 2, Fig. 2). They all arise from the $E_{\text{exc}} < 6.2$ eV levels, for which $b > 1$ in the line-formation layers, while populations of their upper levels are lower than the LTE ones. Therefore, the lines are strengthened in NLTE, and the NLTE abundance corrections, $\Delta_{\text{NLTE}} = \log \epsilon_{\text{NLTE}} - \log \epsilon_{\text{LTE}}$, are negative. However, the NLTE effects

Table 2. NLTE (N) and LTE (L) abundances, $\log \varepsilon$, from lines of Si I and Si II in the Sun and HD 32115.

Transition	λ [Å]	$\log gf$		Sun	HD 32115
Si I					
$4s^3P^\circ - 5p^3P$	5690.42	-1.87 ¹	N	7.64	7.55
$E_{\text{exc}} = 4.93$ eV			L	7.66	7.57
$4s^1P^\circ - 5p^1S$	5772.15	-1.75 ¹	N	7.65	7.60
$E_{\text{exc}} = 5.08$ eV			L	7.67	7.61
$4s^1P^\circ - 5p^1D$	5948.54	-1.23 ¹	N	7.64	7.64
$E_{\text{exc}} = 5.08$ eV			L	7.69	7.67
$3p^3^3D^\circ - 5f^3D$	6142.48	-1.30 ²	N	7.37	7.40
$E_{\text{exc}} = 5.62$ eV			L	7.39	7.41
$3p^3^3D^\circ - 5f^3G$	6155.13	-0.76 ²	N	7.46	7.42
$E_{\text{exc}} = 5.62$ eV			L	7.50	7.44
$3p^3^3D^\circ - 5f^3F$	6237.32	-0.98 ²	N	7.40	7.39
$E_{\text{exc}} = 5.61$ eV			L	7.42	7.41
$3d^1D^\circ - 6f2[7/2]$	6414.98	-1.04 ²	N	7.51	7.51
$E_{\text{exc}} = 5.87$ eV			L	7.53	7.53
$4p^1P - 6d^1D^\circ$	6721.85	-0.94 ³	N	7.36	7.31
$E_{\text{exc}} = 5.86$ eV			L	7.38	7.33
$4p^3D - 6d^3P^\circ$	6741.63	-1.75 ²	N	7.68	7.80
$E_{\text{exc}} = 5.98$ eV			L	7.70	7.83
$4p^1P - 7s(3/2,1/2)^\circ$	6848.58	-1.53 ²	N	7.42	7.32
$E_{\text{exc}} = 5.86$ eV			L	7.43	7.34
$3d^1D^\circ - 5f2[7/2]$	7034.90	-0.88 ²	N	7.64	7.57
$E_{\text{exc}} = 5.87$ eV			L	7.68	7.61
$4p^3D - 7s(3/2,1/2)^\circ$	7373.00	-1.18 ²	N	7.43	7.37
$E_{\text{exc}} = 5.98$ eV			L	7.43	7.39
$3p^3^3D^\circ - 4f^3F$	7405.77	-0.82 ²	N	7.61	7.65
$E_{\text{exc}} = 5.61$ eV			L	7.67	7.70
$4p^1P - 5d^1D^\circ$	7680.27	-0.69 ¹	N	7.65	7.57
$E_{\text{exc}} = 5.86$ eV			L	7.71	7.61
$3d^3F^\circ - 6f2[5/2]$	7849.97	-0.71 ²	N	7.50	7.50
$E_{\text{exc}} = 6.19$ eV			L	7.53	7.53
$4p^3D - 5d^3F^\circ$	7944.00	-0.31 ¹	N	7.62	7.56
$E_{\text{exc}} = 5.98$ eV			L	7.72	7.64
Si II					
$4p^2P^\circ - 4d^2D$	5055.98	0.52 ⁴	N		7.68
$E_{\text{exc}} = 10.07$ eV			L		7.68
$4p^2P^\circ - 5s^2S$	5978.93	0.08 ⁵	N		7.58
$E_{\text{exc}} = 10.07$ eV			L		7.58
$4s^2S - 4p^2P^\circ$	6347.11	0.15 ⁴	N	7.62	7.75
$E_{\text{exc}} = 8.12$ eV			L	7.72	8.04
	6371.37	-0.08 ⁴	N	7.50	7.64
			L	7.58	7.86

Notes. ¹ Garz (1973), ² VALD, ³ Wiese et al. (1969),
⁴ Matheron et al. (2001), ⁵ Blanco et al. (1995).

are small, so that Δ_{NLTE} ranges between -0.02 and -0.06 dex for different lines.

In the hotter, $9380 \leq T_{\text{eff}} \leq 10400$ K, stars, only Si I 3905 Å was measured in the visible spectral range. We note that observed spectra of Vega and HD 145788 do not cover this line. Overionisation of Si I leads to weakened line (Fig. 4) and large positive NLTE abundance correction, which ranges between 0.33 and 0.41 dex for different stars. Si I 3905.523 Å is blending with the Cr II 3905.644 Å line. However, as shown in Fig. 4, a variation of 0.1 dex in the Cr abundance does not influence the derived silicon abundance.

We are lucky to measure five lines of Si I in the UV spectrum of HD 72660 (Table 3). Their NLTE abundances

Table 3. NLTE and LTE abundances, $\log \varepsilon$, from the UV lines of Si I and Si II in HD 72660.

Transition	λ [Å]	E_{exc} [eV]	$\log gf$	NLTE	LTE
Si I					
$3p^3P - 5d^1D^\circ$	1664.51	0.03	-1.80	7.86	7.66
$3p^3P - 5d^3P^\circ$	1666.38	0.00	-1.66	7.84	7.54
$3p^3P - 6s^1P^\circ$	1682.67	0.01	-1.85	7.91	7.64
$3p^3P - 6s^3P^\circ$	1689.29	0.01	-1.83	7.88	7.66
$3p^3P - 4d^3D^\circ$	1699.72	0.03	-2.63	7.82	7.58
Si II					
$3p^2^2D - 5f^2F^\circ$	1710.84	6.86	-0.57	7.97	7.97

Notes. gf -values are from Smith et al. (1987) for Si I,
and from VALD for Si II.

agree well with that from Si I 3905 Å, so that the dispersion in the single line measurements around the mean, $\sigma = \sqrt{\Sigma(\bar{x} - x_i)^2 / (N_i - 1)}$, amounts to 0.04 dex (Table 1). Here, N_i is the number of measured lines. This provides evidence for a reliable abundance from Si I 3905 Å despite blending with Cr II 3905 Å.

4.3.2 Absorption lines of Si II

The Si II multiplets in Table 4 can be separated into three groups with respect to the departures from LTE.

1. Si II 3853-62 Å, 4075-76 Å, 4128-30 Å, 5041-56 Å, and 5957-78 Å. In the model atmospheres with $T_{\text{eff}} \leq 10400$ K, where Si II is a majority species, the lower and upper levels of the corresponding transitions are tightly coupled to the ground state in the line-formation region, below $\log \tau_{5000} \approx -2$ (see Fig. 1). As a result, the NLTE effects are small, Δ_{NLTE} is slightly negative, and does not exceed 0.02 dex for the two bluest multiplets and 0.16 dex for the remaining ones. In the atmospheres of π Cet and ι Her, all these lines are weakened due to overionisation of Si II and the NLTE abundance corrections are positive. For example, they amount to 0.34 to 0.98 dex for different lines in ι Her.

2. Si II 6347, 6371 Å. In the model atmospheres with $T_{\text{eff}} \leq 12800$ K, NLTE leads to strengthened lines (Fig. 5 for 6371 Å) owing to dropping the line source function (S_ν) below the Planck function (B_ν) in the line-formation layers (see Fig. 1). The NLTE effects grow toward higher effective temperature, so that, for Si II 6371 Å, a magnitude of Δ_{NLTE} increases from -0.22 dex in HD 32115 to -0.65 dex in 21 Peg. In the atmosphere of π Cet, overionisation of Si II competes with dropping S_ν/B_ν , however, the latter effect prevails, resulting in $\Delta_{\text{NLTE}} = -0.18$ dex. Overionisation of Si II is the dominant NLTE mechanism in the atmosphere of the hottest star, so that the Si II 6347, 6371 Å lines are greatly weakened and $\Delta_{\text{NLTE}} = 0.60$ and 0.67 dex, respectively.

3. The high-excitation ($E_{\text{exc}} > 12$ eV) lines are observed in the three hottest stars. The exception is Si II 4621.4, 4621.7 Å and 6239 Å in HD 72660, which were measured thanks to the narrower lines compared with that in the other stars of close effective temperature. The high-excitation levels are depopulated in the line-formation layers due to photon loss in the transitions to the low-lying levels in the

Table 4. NLTE (N) and LTE (L) abundances, $\log \varepsilon$, from lines of Si I and Si II in the sample stars.

Transition (E_{exc})	λ [Å]	$\log gf$	Ref	$\log \Gamma_4/N_e$		HD 73666	Vega	HD 72660	HD 145788	Sirius	21 Peg	π Cet	ι Her			
Si I																
$3p^1S_0 - 4s^1P_1$ (1.91 eV)	3905.52	-1.04	O91	-5.60 ¹	N	7.54		7.79		7.59	7.49					
					L	7.16		7.42		7.26	7.08					
Si II																
$3p^2^2D - 4p^2P^o$ (6.86 eV)	3853.67	-1.34	M01	-5.20 ¹	N	7.63				7.67	7.50	7.81	7.85			
					L	7.64				7.66	7.50	7.49	7.25			
					N	7.89				7.84	7.60	7.84	8.03			
					L	7.89				7.84	7.62	7.68	7.48			
$3d^2D - 5p^2P^o$ (9.84 eV)	4075.45	-1.40	M01	-4.89 ²	N	7.94		7.94		7.85	7.69	7.93	7.98			
					L	7.95		7.96		7.85	7.69	7.73	7.37			
					N	7.52		7.78			7.53	7.65	7.67			
					L	7.52		7.77			7.54	7.48	7.33			
$3d^2D - 4f^2F^o$ (9.84 eV)	4128.05	0.36	M01	-4.96 ¹	N	7.53	6.87			7.64		7.48	7.25			
					L	7.59	6.95			7.71		7.47	6.84			
					N	7.54	6.85	7.72		7.59	7.32	7.48	7.15			
					L	7.61	6.93	7.78		7.68	7.48	7.43	6.76			
$4d^2D - 7f^2F^o$ (12.52 eV)	4621.42	-0.61	M95	-3.86 ³	N			7.78			7.50	7.75	b ⁴			
					L			7.76			7.44	7.56				
					N			7.78			7.51	7.75	7.60			
					L			7.76			7.46	7.56	6.95			
$4p^2P^o - 4d^2D$ (10.07 eV)	5041.02	0.03	M01	-4.80 ¹	N	7.85		8.00	7.81	7.88	7.68	7.97	7.94			
					L	7.93		8.06	7.94	7.93	7.80	7.78	6.97			
					N	7.65	6.92	7.77	7.60	7.75	7.45	7.79	7.66			
					L	7.76	6.96	7.86	7.76	7.81	7.60	7.58	6.68			
$4d^2D - 6f^2F^o$ (12.52 eV)	5055.98	0.52	M01	-4.76 ¹	N	7.73		7.85	7.69	7.85	7.56	7.78	7.78			
					L	7.76		7.88	7.74		7.60		6.91			
					N								7.75			
					L								6.57			
$5p^2P^o - 7d^2D$ (12.88 eV)	5466.89	-0.08	M95	-4.20 ³	N							7.88				
					L								7.40			
					N								7.74			
					L								7.60			
$4p^2P^o - 5s^2S$ (10.07 eV)	5469.45	-0.76	M95	-4.06 ³	N							7.88				
					L								7.40			
					N	7.62	6.96	7.71	7.63	7.68	7.36	7.74	7.60			
					L	7.70	7.01	7.77	7.76	7.74	7.46	7.63	6.77			
$4f^2F^o - 6g^2G$ (12.84 eV)	5957.56	-0.22	B95	-4.83 ¹	N	7.55	6.87	7.69	7.57	7.64	7.32	7.63	7.57			
					L	7.65	6.93	7.78	7.74	7.72	7.48	7.57	6.74			
					N			7.85			7.57	7.73	7.92			
					L			7.82			7.41	7.33	e ⁵			
$4s^2S - 4p^2P^o$ (8.12 eV)	6239.61	0.18	M95	-3.54 ³	N							7.77	8.38			
					L								7.99	7.78		
					N	7.60	6.80	7.79	7.55	7.69	7.28	7.77	8.38			
					L	8.20	7.32	8.31	8.14	8.14	8.06	7.99	7.78			
$5p^2P^o - 6d^2D$ (12.88 eV)	6347.11	0.15	M01	-5.08 ¹	N	7.52	6.77	7.75	7.47	7.59	7.24	7.66	8.27			
					L	8.09	7.12	8.15	8.04	7.95	7.89	7.84	7.60			
					N								7.94			
					L								7.94			
$4d^2D - 5f^2F^o$ (12.52 eV)	6818.41	-0.52	M95	-4.24 ³	N							7.78	7.87			
					L								7.34	e		
					N	6829.80	-0.26	M95						7.78	7.87	
					L	6829.83	-1.22	M95						7.34	e	
$4d^2D - 5f^2F^o$ (12.52 eV)	7848.82	0.32	M95	-4.68 ³	N						7.52	7.55	8.36			
					L							7.32	7.14	e		
					N	7849.72	0.47	M95						7.48	7.64	8.29
					L	7849.62	-0.83	M95						7.28	7.23	e

Notes. Γ_4/N_e in rad/s-cm^3 , ¹ Bukvić et al. (2009); ² Wilke (2003, Ph.D. Thesis) as given by Fossati et al. (2009);

³ VALD; ⁴ blend; ⁵ emission line.

Ref. B95 = Blanco et al. (1995), M01 = Matheron et al. (2001), M95 = Mendoza et al. (1995), O91 = O'brian & Lawler (1991).

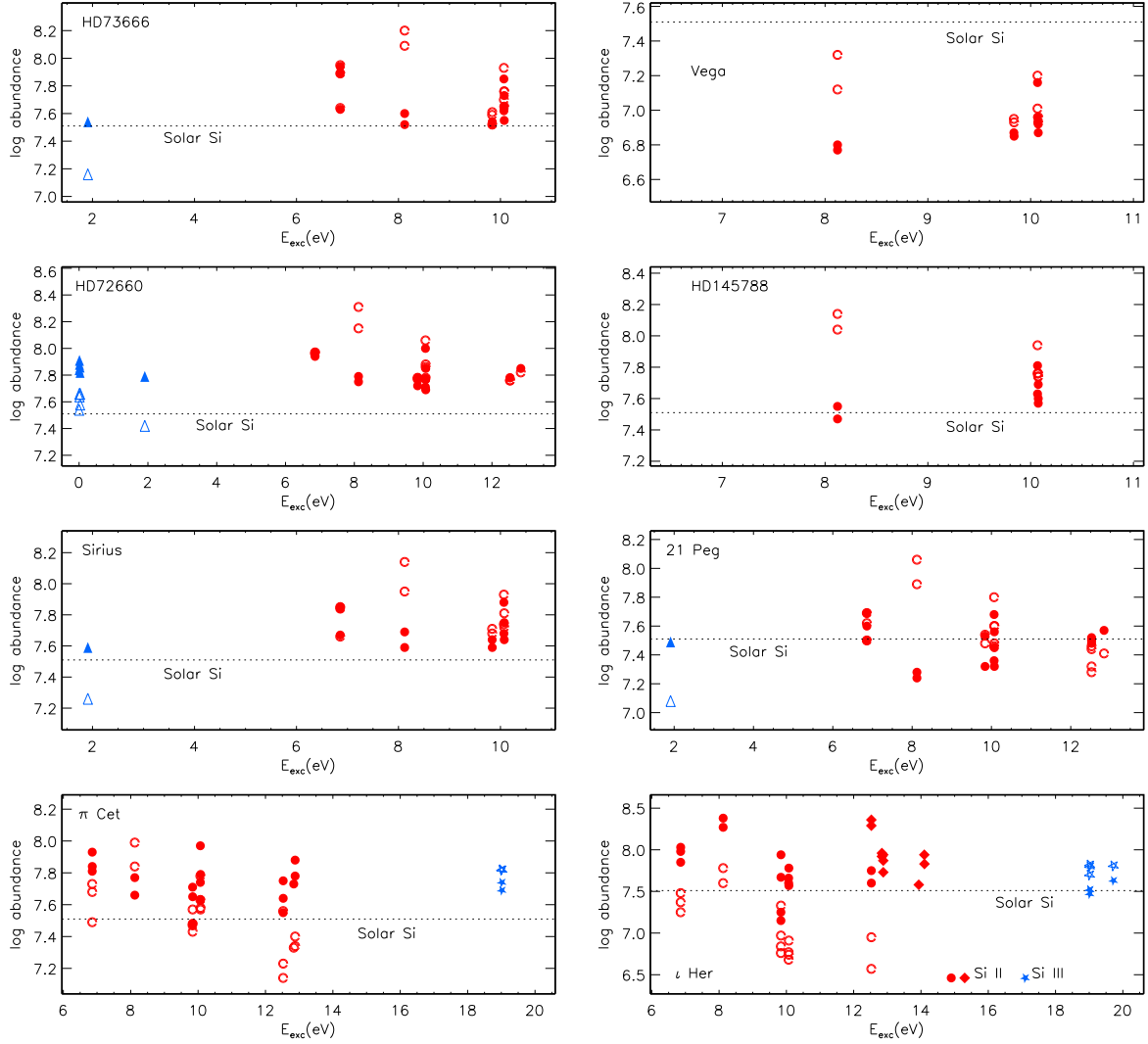


Figure 3. NLTE (filled symbols) and LTE (open symbols) abundances from individual lines of Si I (triangles), Si II (circles), and Si III (5 pointed stars) in the sample stars. For ι Her, the NLTE abundances derived from the Si II emission lines are shown by the rhombi. The dotted line indicates the solar system silicon abundance, $\log \varepsilon_{\odot} = 7.51 \pm 0.01$ (Lodders 2019).

Table 5. NLTE and LTE abundances, $\log \varepsilon$, from lines of Si III in π Cet and ι Her.

λ [Å]	E_{exc} [eV]	$\log gf$	π Cet		ι Her	
			NLTE	LTE	NLTE	LTE
4552.62	19.02	0.29			7.47	7.82
4567.84	19.02	0.07	7.69	7.82	7.52	7.80
4574.76	19.02	-0.41	7.74	7.82	7.52	7.70
5739.73	19.72	-0.10			7.63	7.81

Note. gf -values are from NIST.

$T_{\text{eff}} \leq 10400$ K model atmospheres and due to overionisation of Si II in the hotter atmospheres. For each transition, the lower level is depopulated to a greater extent than is the

upper level, resulting in weakened line compared with its LTE strength (Fig. 6 for 6239 Å). The NLTE effects grow toward higher T_{eff} . For example, for Si II 6239 Å, $\Delta_{\text{NLTE}} = 0.03, 0.16,$ and 0.40 dex for HD 72660, 21 Peg, and π Cet, respectively, and the line appears in emission in ι Her. In this hottest star of our sample, only 4621.7 Å and 5466.8 Å among the high-excitation lines are observed in absorption, although they are greatly weakened by the NLTE effects, with $\Delta_{\text{NLTE}} = 0.65$ and 1.18 dex, respectively. The lines on the long-wave side of 6239 Å either come into emission or disappear. They deserve a special consideration in Sect. 6.3.

4.3.3 Lines of Si III

Observed lines of Si III (Table 5) arise from the transitions $4s^3S - 4p^3P^{\circ}$ ($E_{\text{exc}} = 19.02$ eV) and $4s^1S - 4p^1P^{\circ}$ ($E_{\text{exc}} = 19.72$ eV). In π Cet, only the first multiplet was measured,

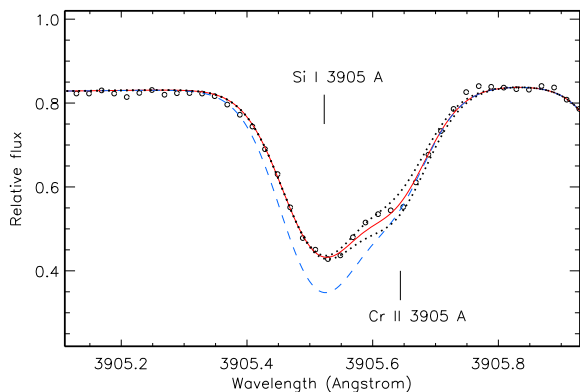


Figure 4. Best NLTE fit (solid curve) of Si I 3905 Å in HD 72660 (open circles). The corresponding LTE line profile is plotted by the dashed curve. The dotted curves show the NLTE synthetic spectra computed with 0.1 dex higher and lower abundance of Cr.

the lines are weak, and form in deep atmospheric layers, around $\log \tau_{5000} \sim -0.1$ (Fig. 1), where the NLTE effects on the lines are caused by slight overpopulation of the lower level relative to its TE population. For Si III 4567 and 4574 Å, $\Delta_{\text{NLTE}} = -0.13$ and -0.08 dex, respectively.

In ι Her, the Si III lines are stronger and form in the layers, where the lower levels of both multiplets have enhanced excitation owing to pumping UV transitions from the low-excitation levels, while the upper levels are depopulated via spontaneous transitions to the low-lying levels. Increasing the line absorption coefficient due to $b_{\text{low}} > 1$ and dropping the line source function below the Planck function due to $b_{\text{up}}/b_{\text{low}} < 1$ result in strengthened lines and negative Δ_{NLTE} of -0.18 to -0.35 dex for different lines.

4.4 Comparison with other NLTE studies

The obtained NLTE abundances can only be compared with the results of Wedemeyer (2001) for lines of Si II in Vega and Nieva & Przybilla (2012) for lines of Si III in ι Her. For the three Si II lines in common, namely, at 4128, 4130, and 5055 Å, the NLTE abundance corrections computed by Wedemeyer (2001) do not exceed 0.11 dex, in absolute value, and agree within 0.03 dex with ours. The NLTE abundances obtained in this study from individual lines of Si III in ι Her agree within 0.03 to 0.08 dex with those of Nieva & Przybilla (2012), and the mean abundances are consistent within 0.04 dex in the two studies.

5 ABUNDANCE ANALYSES OF THE $T_{\text{eff}} \leq 12800$ K STARS

For each of the eight stars with $T_{\text{eff}} \leq 12800$ K, its silicon spectrum is well reproduced in NLTE with a unique element abundance. The star ι Her, with both absorption and emission lines in its spectrum, is discussed in the next section. The average NLTE and LTE abundances from each ionisation stage observed in a given star are presented in Table 1.

We comment on the Si I lines in HD 32115. They reveal a substantial scatter of abundances, with $\sigma = 0.17$ dex,

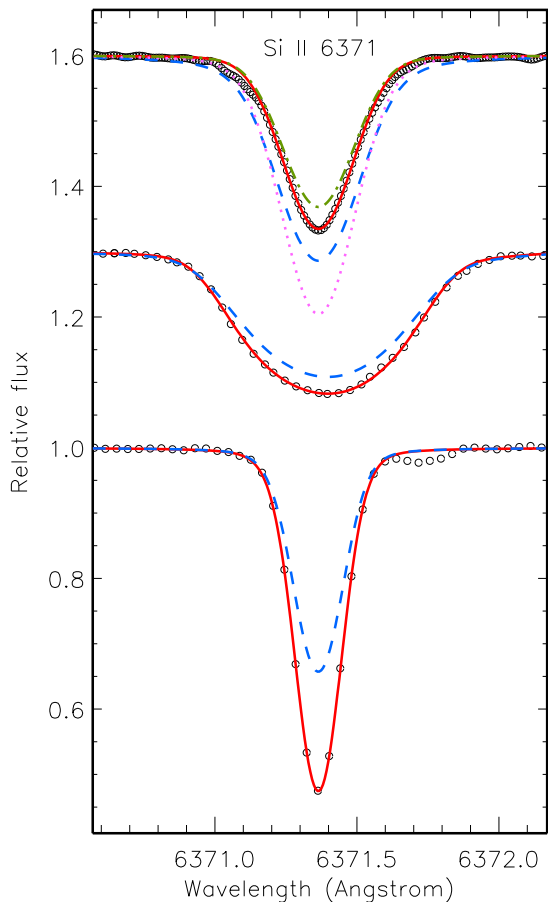


Figure 5. Best NLTE fits (solid curve) of Si II 6371 Å in ι Her, π Cet, and 21 Peg (open circles, from top to down). The corresponding LTE line profiles are plotted by the dashed curves. For ι Her, we also show the NLTE line profiles computed by replacing electron-impact excitation data of Aggarwal & Keenan (2014) with the van Regemorter (1962) approximation for the allowed transitions and $\Upsilon = 1$ for the forbidden transitions (dash-dotted curve) and by replacing the TOPbase photoionisation cross sections for the Si II $4s^2S$, $3d^2D$, and $3p^2^2D$ levels with the hydrogenic ones (dotted curve). For better visibility, spectra of π Cet and ι Her are shifted along Y axis.

independent of either LTE or NLTE and independent of either measured equivalent widths (Fig. 2) or excitation potentials. Such a scatter is, most probably, due to the uncertainties in gf -values. Indeed, the dispersion was substantially reduced, down to $\sigma = 0.06$ dex, in a line-by-line differential approach, where from stellar line abundances we subtracted individual abundances of their solar counterparts. The solar abundances (Table 2) were derived using the Kitt Peak Solar Flux Atlas (Kurucz et al. 1984) and the calculations with the MARCS model atmosphere 5777/4.44/0 (Gustafsson et al. 2008) and a depth-independent microturbulence of 0.9 km s^{-1} .

For Si II in each star, NLTE reduces substantially the line-to-line scatter compared with the LTE case. For example, from $\sigma = 0.24$ to 0.08 dex for HD 32115 (four Si II lines) and from $\sigma = 0.25$ to 0.14 dex for π Cet (19 lines).

The NLTE line formation is essential for achieving con-

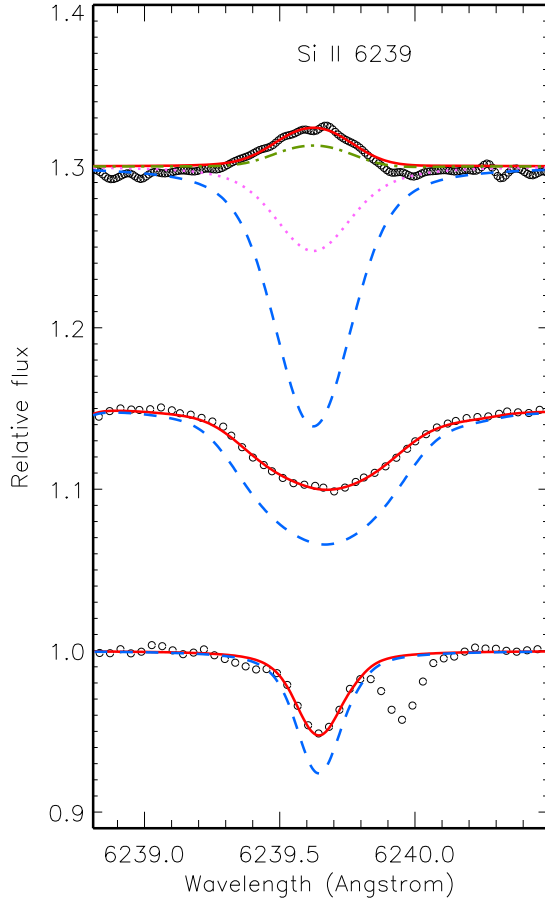


Figure 6. The same as in Fig. 5 for Si II 6239 Å.

sistent abundances from Si I and Si II in the five stars, where lines of both ionisation stages were measured. For example, the abundance difference (Si I – Si II) = –0.07 and –0.21 dex in NLTE and LTE, respectively, for HD 32115, and the corresponding numbers are –0.01 and –0.54 dex for 21 Peg. Fairly consistent NLTE abundances from lines of Si II and Si III were found in π Cet, while, in LTE, the abundance difference amounts to –0.23 dex.

The [Si/H] values were computed using the solar Si abundance, $\log \varepsilon_{\odot} = 7.51 \pm 0.01$, as recommended by [Lodders \(2019\)](#). For stellar Si abundance, we computed the average value, if silicon was observed in the two ionisation stages. The exception is Sirius. We relied on its Si II based abundance, having in mind that the only measured Si I line is affected by the Cr II line (see Fig. 4 for HD 72660) and Sirius is an Am star. We obtained that the silicon abundance follows the iron one in our sample stars, including a λ Boo star Vega and the three Fe-rich stars, but except for π Cet. This suggests that the mechanisms, which produced deviations in metal abundances of our chemically peculiar stars from the solar one, did not separate chemical elements. For π Cet, with [Fe/H] = 0, according to [Fossati et al. \(2009\)](#), we found a supersolar abundance of [Si/H] = 0.23 from lines of both ionisation stages, Si II and Si III.

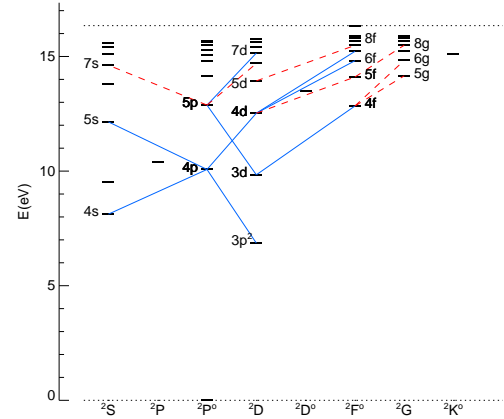


Figure 7. The doublet terms in the model atom of Si II. The absorption and emission spectral lines observed in ι Her arise from the transitions shown as continuous and dashed lines, respectively.

6 NLTE ANALYSIS OF ι HER

6.1 Silicon absorption lines

NLTE reduces σ of the Si II based abundance, however, the line-to-line scatter remains uncomfortably large (Fig. 3). It is largely contributed by lines of the two multiplets, 3853–62 Å ($E_{\text{exc}} = 6.86$ eV) and 6347–71 Å ($E_{\text{exc}} = 8.12$ eV). For example, for Si II in NLTE, we obtained $\sigma = 0.50$ dex, when taking Si II 6347–71 Å into account, and $\sigma = 0.25$ dex without these two lines. In order to be consistent with the other lines, Si II 6347 and 6371 Å need to be strengthened in NLTE like that shown in Fig. 5 for a model, where the TOPbase photoionisation cross sections were replaced with the hydrogenic ones for the Si II 4s, 3d, and $3p^2\ ^2D$ levels. Such a change in the NLTE effects compared with that for our standard model atom can be understood. From inspecting the NET = $n_l R_{lu} - n_u R_{ul}$ rates for b–f transitions of Si II, it was found that overionisation of exactly these three levels is the main driver of overall overionisation of Si II. Here, R_{lu} and R_{ul} are radiative rates of the $l-u$ and the reverse transitions, respectively. For the Si II 4s and 3d levels, their hydrogenic photoionisation cross sections are smaller than the TOPbase ones, by more than one order of magnitude near the thresholds. Therefore, their use results in weakened NLTE effects for Si II and fits better to Si II 6347, 6371 Å. However, with such an atomic model, we cannot reproduce the Si II emission lines (see Sect. 6.3).

Even without these two lines, the Si II based abundance is higher than that from the Si III lines, by 0.20 dex. For comparison, under the LTE assumption, an abundance difference between Si II and Si III amounts to –0.72 dex. When relying on the Si III lines, close-to-solar silicon abundance of [Si/H] = 0.03 ± 0.07 was obtained for ι Her, in line with the earlier determinations of [Nieva & Przybilla \(2012\)](#).

6.2 Uncertainties in derived abundances

We checked a sensitivity of the NLTE abundances from representative lines of Si II and Si III to variations in atomic

Table 6. Error estimates for the NLTE calculations of the silicon lines in ι Her.

	Changes in $\log \epsilon_{\text{Si}}$ (dex)					
	Si II				Si III	
	3856 Å	5978 Å	6239 Å	6371 Å	4567 Å	
Atmospheric parameters:						
$T_{\text{eff}} - 200$ K	$\sigma_{T_{\text{eff}}}$	-0.02	-0.05	+0.07	-0.06	+0.06
$\log g + 0.05$	$\sigma_{\log g}$	-0.02	-0.01	+0.02	-0.01	+0.04
$\xi_t + 0.5$ km s $^{-1}$	σ_{ξ}	-0.08	-0.01	0.00	-0.06	-0.04
Line data: $\Gamma_4 * 0.5$	σ_{Γ}	+0.05	+0.01	0.00	+0.04	+0.05
Photoionisations:						
cross sections * 1.1	σ_{RBF}	0.00	-0.01	+0.01	0.00	0.00
cross sections * 2		-0.02	-0.03	+0.02	-0.01	0.00
Si II $3p^2P^\circ - 3p^2D$, $3p^2S$, $4s^2S$ transitions:						
$f_{lu} * 10$		+0.16	-0.04	+0.03	-0.33	0.00
Collisional transitions:						
(Y and C_{vR}) * 2		-0.01	+0.03	abs	0.00	0.00
(Y and C_{vR}) * 0.5	σ_{CBB}	+0.01	-0.05	-0.50	0.00	0.00
(Y , C_{vR} , and C_{AK}) * 2		-0.02	-0.03	abs	-0.07	0.00
Δ_{NLTE}		0.55	0.83	e	0.67	-0.28

Notes. C_{vR} = van Regemorter (1962) rates; C_{AK} = Aggarwal & Keenan (2014) rates; abs = absorption is predicted; e = emission line; 0.00 means smaller than 0.01, in absolute value.

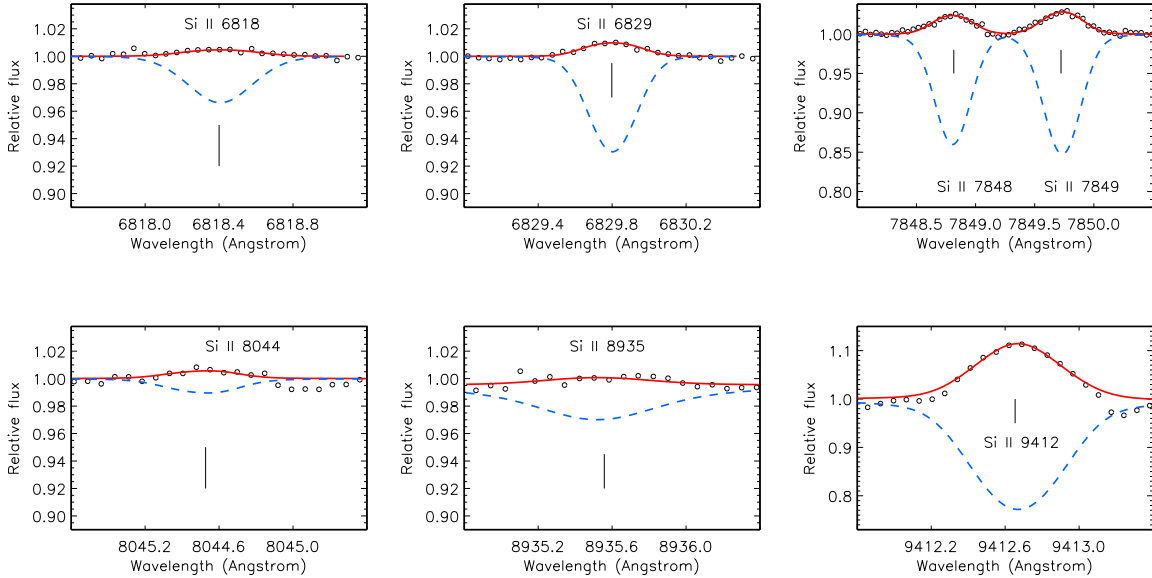


Figure 8. Best NLTE fits (solid curves) of the emission Si II lines in ι Her (open circles). The obtained Si abundances are presented in Table 4. The corresponding LTE line profiles are shown by dashed curves.

model and atmospheric parameters. Table 6 summarises results of our tests.

The NLTE effects for Si II 6347, 6371 Å were found to be rather stable. Variations in photoionisation cross sections and collisional rates produce abundance shifts of up to 0.07 dex. A substantial reduction of Δ_{NLTE} , by 0.33 dex, was obtained in the only case, where oscillator strengths of the pumping $3p^2P^\circ - 3p^2D$ (1808-17 Å), $3p^2S$ (1304-09 Å), and $4s^2S$ (1526-33 Å) transitions were increased by a fac-

tor of 10. Such a big uncertainty in f_{lu} is unlikely. We shall conclude that we are not able to treat correctly the formation of Si II 6347, 6371 Å in ι Her. These two lines were not accounted for, when computing the mean abundance from the Si II lines.

Nieva & Przybilla (2012) estimate the uncertainties in T_{eff} , $\log g$, and ξ_t as 200 K, 0.05 dex, and 1 km s $^{-1}$, respectively. A downward revision of T_{eff} would reduce the mean abundance from lines of Si II, by 0.03 dex, and, in contrast,

Table 7. Emission lines of Si II in ι Her.

Transition	E_{exc} [eV]	λ [Å]	$\log gf$	$\log \epsilon$ NLTE
$4f^2F^\circ - 6g^2G$	12.84	6239.61	0.18	7.92
		6239.61	-1.12	
$5p^2P^\circ - 6d^2D$	12.88	6239.66	0.02	
		6818.41	-0.52	7.94
		6829.80	-0.26	7.87
$4d^2D - 5f^2F^\circ$	12.52	6829.83	-1.22	
		7848.82	0.32	8.36
		7849.72	0.47	8.29
$5p^2P^\circ - 7s^2S$	12.88	7849.62	-0.83	
		7125.85	-0.79	7.73
		7911.52	-0.42	7.83
$5f^2F^\circ - 9g^2G$	14.10	7911.63	-0.60	
		8044.41	-0.59	7.58
$5d^2D - 8f^2F^\circ$	13.94	8044.55	-0.44	
		8935.50	-0.12	7.94
$5f^2F^\circ - 8g^2G$	14.10	8935.63	-0.30	
		9412.66	1.23	7.96
		9412.66	-0.31	
$4f^2F^\circ - 5g^2G$	12.84	9412.78	1.12	

Notes. See text for sources of gf -values.

would increase the mean abundance for Si III, by 0.08 dex, removing, in part, a discrepancy between Si II and Si III. Upward revision of $\log g$ would act in the same direction, however, the abundance shifts are smaller.

For the majority of the Si II lines in ι Her, we use the Γ_4/N_e values from laboratory measurements of Bukvić et al. (2009). They are proven to work well for the stars (Sect. 5), where the quadratic Stark effect broadening is stronger than for ι Her. While approximate formula of Cowley (1971) was applied for lines of Si III. A reduction of Γ_4 by a factor of two would increase the Si III based abundance, by 0.05 dex (Table 6).

Thus, the obtained abundance difference between Si II (without 6347, 6371 Å) and Si III can arise due to the uncertainties in atmospheric parameters and line data.

6.3 Origin of Si II emission lines

Ten lines of Si II, which arise from the transitions between the high-excitation doublet terms (Fig. 7), reveal emission or disappear in spectrum of ι Her. They are listed in Table 7 and, in part, are displayed in Figs. 6 and 8. Their gf -values are based on calculations of Mendoza et al. (1995), as presented by NIST. An exception is the Si II 9412 Å triplet. NIST provides $\log gf = -0.306$ for the only line, which arises from the transition between the $J_{\text{low}} = 7/2$ and $J_{\text{up}} = 7/2$ sublevels. In order to obtain gf -values given in Table 7, we used calculations of R. Kurucz for all three lines of this triplet, as available in VALD: $\log gf = 1.012$ ($7/2 - 9/2$), -0.532 ($7/2 - 7/2$), and 0.899 ($5/2 - 7/2$) and applied their gf ratios to the known NIST value.

The detected emission features are of photospheric origin and naturally explained by interlocked NLTE effects acting in a photosphere, like to emission lines of C I (Alexeeva et al. 2016) and Ca II (Sitnova et al. 2018) in

ι Her. The main driving mechanism of emission is overionisation of Si II. As shown in Fig. 1 (bottom panel), the lower level of each emission transition is depopulated to the greater extent than is the upper level in the line-formation layers, resulting in a line source function which rises relative to the local Planck function with photospheric height. It is essential that the NLTE correction to stimulated emission is sensitive to small deviations of the departure coefficients from unity whenever $h\nu \ll kT$. This explains why in the transitions from common lower level, $4d$, the shorter wavelength lines, at 4621 and 5466 Å, appear in absorption, although being greatly weakened compared with their LTE strengths, while the near-IR lines at 7848, 7849 Å are in emission.

We checked how the emission mechanism is stable with respect to a variation in atomic data. Table 6 shows the abundance shifts for Si II 6239 Å in a part of all the tests made. Increasing photoionisation cross sections within their uncertainties (10 % for the TOPbase data) and even twice has minor effect on the emission phenomenon. The effect is strong, so that emission in the Si II lines disappear, when the TOPbase photoionisation cross sections are either reduced by a factor of 10 or replaced, in part (for the Si II $4s$, $3d$, and $3p^2^2D$ levels, Fig. 6) with the hydrogenic ones.

Another set of test calculations was performed by varying collisional recipes: (i) electron-impact excitation data of Aggarwal & Keenan (2014) were replaced with the van Regemorter (1962) semi-empirical approximation for the allowed transitions and $\Upsilon = 1$ for the forbidden transitions (Fig. 6 for Si II 6239 Å); (ii) and (iii) the electron-impact ionisation rates were scaled by a factor of 0.1 and 10; (iv) for each b-b transition, its collisional rate was scaled by a factor of 2; (v), (vi), and (vii) for the transitions missing in Aggarwal & Keenan (2014), the van Regemorter (1962) rates and the standard $\Upsilon = 1$ value were scaled by a factor of 0.1, 0.5, and 2. Results of the tests (iv), (vi), and (vii) for Si II 6239 Å are given in Table 6. Emission in Si II 6239 Å disappear, if either to decrease the electron-impact ionisation rates (ii), or to increase the electron-impact excitation rates (iv, vii). The remaining tests keep emission in the Si II lines, although the best line profile fits are achieved with different element abundances for different collisional recipes.

Using our standard model atom, we derived the NLTE abundances from fitting the emission line profiles (Table 7 and Fig. 3). They lie between $\log \epsilon = 7.58$, which is close to the Si III based abundance, and substantially higher value of $\log \epsilon = 8.36$. Our test calculations show that a magnitude of emission is very sensitive to a variation in collisional rates for the high-excitation transitions. Exactly those transitions are missing in calculations of Aggarwal & Keenan (2014) that include the levels below $5p^2P^\circ$. Extended calculations of electron-impact excitation cross sections for Si II are highly desirable for achieving consistent abundances from different emission lines.

Sadakane & Nishimura (2019) registered 12 emission lines of Si II in ι Her. Our NLTE calculations reproduce ten of them (Table 7). For the remaining two lines, at 5688 and 5701 Å, the NLTE calculations predict too strong emission. In order to fit to the observations, one needs to reduce the Si abundance compared with the solar value, by more than one order of magnitude. Both lines arise from the transition $3p3d^4F^\circ - 3p4p^4D$, with $E_{\text{exc}} > 14$ eV for the lower level. The majority of the quartet atomic terms have energies higher

Table 8. NLTE abundance corrections (dex) for lines of Si I in the grid of model atmospheres.

λ [Å]	T_{eff} [kK], $\log g = 4.0$		
	7	8	9
5948	-0.04	0.02	0.46
6155	-0.03	-0.00	0.16
7405	-0.05	-0.01	0.24

This table is available in its entirety in a machine-readable form in the online journal. A portion is shown here for guidance regarding its form and content.

than the ionisation energy of the Si II ground state, so that our model atom includes a few number (seven) of quartet terms. These levels are weakly coupled to the doublet terms, mostly via collisional processes, and their populations are more dependent of the transitions between the quartet levels. Since the system of quartet terms in our model atom is certainly incomplete, we cannot compute their populations correctly. For example, our NLTE calculations predict emission for the multiplet 6665, 6671, 6699 Å ($3p4s^4P^o - 3p4p^4D$), while these lines are observed in absorption.

7 NLTE ABUNDANCE CORRECTIONS DEPENDING ON ATMOSPHERIC PARAMETERS

Our analyses of the silicon lines in the nine stars with well determined atmospheric parameters provide evidence for a correct treatment of the NLTE line formation for Si I-II-III through a range of A-B spectral types. Therefore, we can recommend the users to apply in their research the NLTE abundance corrections computed in this study. They are available for the lines listed in Tables 2 (Si I), 4 (Si I 3905 Å and Si II), and 5 (Si III). For calculations of Δ_{NLTE} , the model atmospheres with solar metallicity and $\log g = 3.5, 4.0, \text{ and } 4.5$ were taken from the Kurucz's grid⁷. For Si I, Si II, and Si III, T_{eff} varies between 7000 and 9000 K, 7000 and 20000 K, and 12000 and 20000 K, respectively, with a step of 1000 K. Tables 8 and 9 and Fig. 9 present, in part, the computed Δ_{NLTE} .

For the lines lying in the wings of the hydrogen lines, that is, Si I 3905 Å, Si II 3853, 3856, 3862, 4075, 4076, 4128, and 4130 Å, we recommend to determine abundances from the NLTE spectral synthesis method, but not simply adding the NLTE corrections to the LTE abundances. Our Δ_{NLTE} for Si II 6347, 6371 Å should be applied with a caution in case of the stars as hot as ι Her (see Sect. 6.3).

8 CONCLUSIONS

This paper presents a new comprehensive model atom of Si I-II-III that can be applied to the NLTE analyses of Si I,

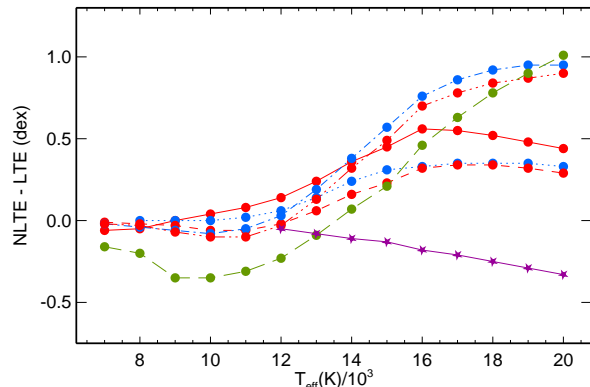


Figure 9. NLTE abundance corrections for Si II lines (circles) and Si III 4567 Å (5 pointed stars) depending on T_{eff} in the models with common $\log g = 4.0$ and solar metallicity. Different type curves correspond to different lines of the Si II: 3862 Å (solid), 4075 Å (dotted), 4128 Å (short-dashed), 5055 Å (dot-dashed), 5978 Å (three-dot-dashed), and 6371 Å (long-dashed).

Si II, and Si III lines in a wide range of spectral types, where they are observed. Here, we performed the NLTE calculations for a range of atmospheric parameters characteristic of unevolved A-B type stars: $T_{\text{eff}} = 7000$ to $20\,000$ K, $\log g = 3.5, 4.0, 4.5$, and solar metallicity. The NLTE effects are different for lines of different ions in a given model atmosphere, and they depend strongly on T_{eff} .

For lines of Si I, the NLTE effects are small for $T_{\text{eff}} \leq 8000$ K, with slightly negative Δ_{NLTE} at $T_{\text{eff}} = 7000$ K and slightly positive ones at $T_{\text{eff}} = 8000$ K. The $E_{\text{exc}} > 4.9$ eV lines are steeply weakened with increasing T_{eff} and most of them cannot be measured in the $T_{\text{eff}} \sim 9000$ K stars. For the strongest of them and Si I 3905 Å, Δ_{NLTE} grows towards higher T_{eff} and reaches 0.42 dex for Si I 3905 Å in the 13000/4.0 model atmosphere.

The first ion of silicon is a majority species in the line formation layers of the $T_{\text{eff}} \leq 11\,000$ K models and is subject to overionisation in the hotter atmospheres. Except for Si II 6347, 6371 Å, the NLTE effects are small for the Si II lines, where Si II is a majority species. For different lines, Δ_{NLTE} can be of different sign in a given atmosphere and does not exceed 0.1 dex, in absolute value. The same lines in the $T_{\text{eff}} \geq 12\,000$ K models are weakened compared with their LTE strengths due to overionisation of Si II, resulting in positive Δ_{NLTE} , which grow with increasing T_{eff} . For the Si II 3853-62 Å, 4075-76 Å, and 4128-30 Å multiplets, Δ_{NLTE} reach their maximal values at T_{eff} of about 17000 K and decrease for higher T_{eff} due to shifting the line formation depths to deeper atmospheric layers. The NLTE effects are, in particular, large for the Si II 5041-56 Å and 5957-78 Å multiplets, with Δ_{NLTE} of up to 0.95 dex in the 20000/4.0 model.

The Si II 6347, 6371 Å lines are strongly strengthened in NLTE over wide range of T_{eff} , even in the atmospheres, where Si II is subject to overionisation. For example, for Si II 6347 Å in the $\log g = 4.0$ models, Δ_{NLTE} reaches the most negative value of -0.40 dex for $T_{\text{eff}} = 9000$ and 10000 K and turns to positive for $T_{\text{eff}} \geq 14000$ K.

Our NLTE calculations predict that, in the $T_{\text{eff}} \geq 17000$ K models, some lines of Si II, which arise from the

⁷ <http://kurucz.harvard.edu/grids/gridp00odfnew/>

Table 9. NLTE abundance corrections (dex) for lines of Si I, Si II, and Si III in the grid of model atmospheres.

λ [Å]	T_{eff} [kK], $\log g = 4.0$													
	7	8	9	10	11	12	13	14	15	16	17	18	19	20
Si I														
3905	-0.01	0.03	0.34	0.43	0.36	0.39	0.42							
Si II														
5978	-0.02	-0.03	-0.07	-0.10	-0.10	-0.03	0.13	0.32	0.49	0.70	0.78	0.84	0.87	0.90
6239			0.05	0.07	0.14	0.27	0.54	1.07	1.12	1.17	e	e	e	
6371	-0.16	-0.20	-0.35	-0.35	-0.31	-0.23	-0.09	0.07	0.21	0.46	0.63	0.78	0.90	1.01
Si III														
4567						-0.05	-0.08	-0.11	-0.13	-0.18	-0.21	-0.25	-0.29	-0.33

For a given line, Δ_{NLTE} is provided, if the NLTE equivalent width exceeds 3 mÅ. e = emission line.

This table is available in its entirety in a machine-readable form in the online journal. A portion is shown here for guidance regarding its form and content.

high-excitation (above $4d^2D$) doublet levels, come into emission due to the NLTE effects acting in an atmosphere. The main driving mechanism of emission is overionisation of Si II.

NLTE abundance corrections for the Si III lines are negative in the stellar parameter range, with which we concern, and they increase, in absolute value, toward higher T_{eff} .

The new model atom was tested with nine unevolved A9 to B3-type stars, with well determined atmospheric parameters and high-resolution observed spectra available. The hottest star, ι Her, is known by many emission lines of various chemical species, including 12 lines of Si II (Sadakane & Nishimura 2019). Our NLTE calculations with a classical hydrostatic model that represents the atmosphere of ι Her reproduced ten of them, although using rather different element abundances for different lines. A magnitude of emission is sensitive to a variation in collisional rates. Accurate electron-impact excitation cross sections for the Si II transitions between the high-excitation levels are highly desirable, in order to achieve consistent abundances from different emission lines.

For each star, the NLTE and LTE abundances were determined from the absorption lines. NLTE reduces substantially the line-to-line scatter for Si II compared with the LTE case and leads to consistent mean abundances from lines of different ionisation stages. For example, in NLTE and LTE, the Si I – Si II abundance difference in 21 Peg amounts to -0.01 and -0.54 dex, respectively, and the Si II – Si III difference in ι Her is $+0.20$ and -0.72 dex. Thus, with the new model atom, the line formation for Si I – Si II – Si III in atmospheres of A to mid B-type stars is treated correctly. The exception is the Si II 6347, 6371 Å doublet in ι Her, for which the NLTE effects are overestimated. They are stable with respect to variations in photoionisation cross sections and electron-impact excitation data. At this stage, we failed to understand this problem and further theoretical work is required.

We obtained that, except for π Cet, the silicon abundance follows the iron one in our sample stars, including a λ Boo star Vega and Am stars HD 72660 and Sirius. This suggests that the mechanisms, which produced deviations in metal abundances of our chemically peculiar stars from the solar one, did not separate chemical elements. A supersolar

abundance of $[\text{Si}/\text{H}] = 0.23$ was found from lines of the two ionisation stages, Si II and Si III, for π Cet, which has $[\text{Fe}/\text{H}] = 0$, according to Fossati et al. (2009). A NLTE study of the iron lines in A to mid B-type stars is in progress (Sitnova et al., in prep.)

Acknowledgments. The author thanks K.M. Aggarwal for providing effective collision strengths for the Si II transitions, T. Ryabchikova for providing the observed spectra and the model atmospheres computed with the code LLMODELS, and J. Landstreet for providing the UV spectrum of HD 72660. This study made use of the ESO UVESPOP, NIST, TOPbase, NORAD, open-ADAS⁸, VALD, ADS⁹, and R. Kurucz’s databases.

REFERENCES

- Aggarwal K. M., Keenan F. P., 2014, *MNRAS*, **442**, 388
 Alexeeva S. A., Ryabchikova T. A., Mashonkina L. I., 2016, *MNRAS*, **462**, 1123
 Alexeeva S., Ryabchikova T., Mashonkina L., Hu S., 2018, *ApJ*, **866**, 153
 Amarsi A. M., Asplund M., 2017, *MNRAS*, **464**, 264
 Bailey J. D., Landstreet J. D., 2013, *A&A*, **551**, A30
 Bard S., Carlsson M., 2008, *ApJ*, **682**, 1376
 Becker S. R., Butler K., 1990, *A&A*, **235**, 326
 Bergemann M., Kudritzki R.-P., Würl M., Plez B., Davies B., Gazak Z., 2013, *ApJ*, **764**, 115
 Blanco F., Botho B., Campos J., 1995, *Phys. Scr.*, **52**, 628
 Bukvić S., Djeniže S., Srećković A., 2009, *A&A*, **508**, 491
 Butler K., Giddings J., 1985, Newsletter on the analysis of astronomical spectra, No. 9, University of London
 Castelli F., Kurucz R. L., 1993, in Dworetzky M. M., Castelli F., Faraggiana R., eds, *Astronomical Society of the Pacific Conference Series Vol. 44, IAU Colloq. 138: Peculiar versus Normal Phenomena in A-type and Related Stars*. p. 496
 Cowley C. R., 1971, *The Observatory*, **91**, 139
 Cunto W., Mendoza C., Ochsenbein F., Zeippen C. J., 1993, *A&A*, **275**, L5
 Fernández-Mencheró L., Del Zanna G., Badnell N. R., 2014, *A&A*, **572**, A115

⁸ <http://open.adas.ac.uk>

⁹ http://adsabs.harvard.edu/abstract_service.html

- Finn G. D., McAllister H. C., 1978, *Sol. Phys.*, **56**, 263
- Fossati L., Bagnulo S., Monier R., Khan S. A., Kochukhov O., Landstreet J., Wade G., Weiss W., 2007, *A&A*, **476**, 911
- Fossati L., Ryabchikova T., Bagnulo S., Alecian E., Grunhut J., Kochukhov O., Wade G., 2009, *A&A*, **503**, 945
- Fossati L., Ryabchikova T., Shulyak D. V., Haswell C. A., Elmasli A., Pandey C. P., Barnes T. G., Zwintz K., 2011, *MNRAS*, **417**, 495
- Garz T., 1973, *A&A*, **26**, 471
- Golriz S. S., Landstreet J. D., 2016, *MNRAS*, **456**, 3318
- Gustafsson B., Edvardsson B., Eriksson K., Jorgensen U. G., Nordlund Å., Plez B., 2008, *A&A*, **486**, 951
- Hill G. M., Landstreet J. D., 1993, *A&A*, **276**, 142
- Hubeny I., Hummer D. G., Lanz T., 1994, *A&A*, **282**, 151
- Hummer D. G., Mihalas D., 1988, *ApJ*, **331**, 794
- Kamp L. W., 1978, *ApJS*, **36**, 143
- Kramida A., Ralchenko Y., Reader J., Team N. A., 2019, NIST Atomic Spectra Database (version 5.7.1). USA, <http://physics.nist.gov/asd>
- Kurucz R. L., Furenlid I., Brault J., Testerman L., 1984, Solar flux atlas from 296 to 1300 nm. New Mexico: National Solar Observatory
- Lennon D. J., Brown P. J. F., Dufton P. L., Lynas-Gray A. E., 1986, *MNRAS*, **222**, 719
- Lodders K., 2019, arXiv e-prints, p. [arXiv:1912.00844](https://arxiv.org/abs/1912.00844)
- Martin W. C., Zalubas R., 1983, *Journal of Physical and Chemical Reference Data*, **12**, 323
- Matheron P., Escarguel A., Redon R., Lesage A., Richou J., 2001, *J. Quant. Spectrosc. Radiative Transfer*, **69**, 535
- Mendoza C., Eissner W., LeDourneuf M., Zeippen C. J., 1995, *Journal of Physics B Atomic Molecular Physics*, **28**, 3485
- Mihalas D., Hummer D. G., Conti P. S., 1972, *ApJ*, **175**, L99
- Nahar S. N., 1995, *ApJS*, **101**, 423
- Nahar S. N., 2000, *ApJS*, **126**, 537
- Nayfonov A., Däppen W., Hummer D. G., Mihalas D., 1999, *ApJ*, **526**, 451
- Nieva M.-F., Przybilla N., 2012, *A&A*, **539**, A143
- O'brian T. R., Lawler J. E., 1991, *Phys. Rev. A*, **44**, 7134
- Przybilla N., Nieva M.-F., Butler K., 2008, *ApJ*, **688**, L103
- Przybilla N., Nieva M.-F., Butler K., 2011, *Journal of Physics Conference Series*, **328**, 012015
- Ryabchikova T., Piskunov N., Kurucz R. L., Stempels H. C., Heiter U., Pakhomov Y., Barklem P. S., 2015, *Phys. Scr.*, **90**, 054005
- Sadakane K., Nishimura M., 2017, *PASJ*, **69**, 48
- Sadakane K., Nishimura M., 2019, *PASJ*, **71**, 45
- Seaton M. J., 1962, in Bates D. R., ed., Atomic and Molecular Processes. p. 375
- Seaton M. J., 1987, *Journal of Physics B Atomic Molecular Physics*, **20**, 6363
- Shchukina N., Sukhorukov A., Trujillo Bueno J., 2012, *ApJ*, **755**, 176
- Shi J. R., Gehren T., Butler K., Mashonkina L. I., Zhao G., 2008, *A&A*, **486**, 303
- Shulyak D., Tsymbal V., Ryabchikova T., Stütz C., Weiss W. W., 2004, *A&A*, **428**, 993
- Singh J., Aggarwal S., Jha A. K. S., Singh A. K., Mohan M., 2011, *Canadian Journal of Physics*, **89**, 1119
- Sitnova T. M., Mashonkina L. I., Ryabchikova T. A., 2013, *Astronomy Letters*, **39**, 126
- Sitnova T. M., Mashonkina L. I., Ryabchikova T. A., 2016, *MNRAS*, **461**, 1000
- Sitnova T. M., Mashonkina L. I., Ryabchikova T. A., 2018, *MNRAS*, **477**, 3343
- Smith P. L., Huber M. C. E., Tozzi G. P., Griesinger H. E., Cardon B. L., Lombardi G. G., 1987, *ApJ*, **322**, 573
- Tsymbal V., Ryabchikova T., Sitnova T., 2019, in Kudryavtsev D. O., Romanyuk I. I., Yakunin I. A., eds, Astronomical Society of the Pacific Conference Series Vol. 518, Astronomical Society of the Pacific Conference Series. pp 247–252
- Vernazza J. E., Avrett E. H., Loeser R., 1976, *ApJS*, **30**, 1
- Wedemeyer S., 2001, *A&A*, **373**, 998
- Wiese W. L., Smith M. W., Miles B. M., 1969, Atomic transition probabilities. Vol. 2: Sodium through Calcium. A critical data compilation
- van Regemorter H., 1962, *ApJ*, **136**, 906